Supplementary materials

Fig S1. Functional activation of ROI in sensorimotor areas of unaffected hemisphere.

Fig. S2. Effect sizes of functional correlations.

Fig. S3. Distribution of the adjusted *P* values for the whole-brain functional connectivity analysis comparison to phantom sensation during task.

Fig. S4. Correlations for ROI-to-ROI connectivity.

Fig. S5. Correlations for network-to-network connectivity.

Fig. S6. Residual limb muscle activation during task.

Fig. S7. ROI segmentation.

Fig. S8. Quality control histograms of motion correction parameter values across all participants.

Fig. S9. Quality assurance plot of denoising.

Table S1. Subject demographics

Table S2. Individual subject data for functional activation and neuromuscular characteristics

“Agonist-antagonist myoneural interface amputation preserves proprioceptive sensorimotor neurophysiology in lower limbs”

Supplemental Materials

Shriya S. Srinivasan[1,2,3], Greta Tuckute[2], Jasmine Zou[2], Samantha Gutierrez-Arango[2,3], Hyungeun Song[1,2,3], Robert L. Barry[1,3,4] & Hugh Herr[2]

[1] Harvard-MIT Program in Health Sciences and Technology, Massachusetts Institute of Technology, Cambridge, Massachusetts, USA
[2] MIT Center for Extreme Bionics, Massachusetts Institute of Technology, Cambridge, Massachusetts, USA
[3] Athinoula A. Martinos Center for Biomedical Imaging, Department of Radiology, Massachusetts General Hospital, Charlestown, Massachusetts, USA
[4] Department of Radiology, Harvard Medical School, Boston, Massachusetts, USA

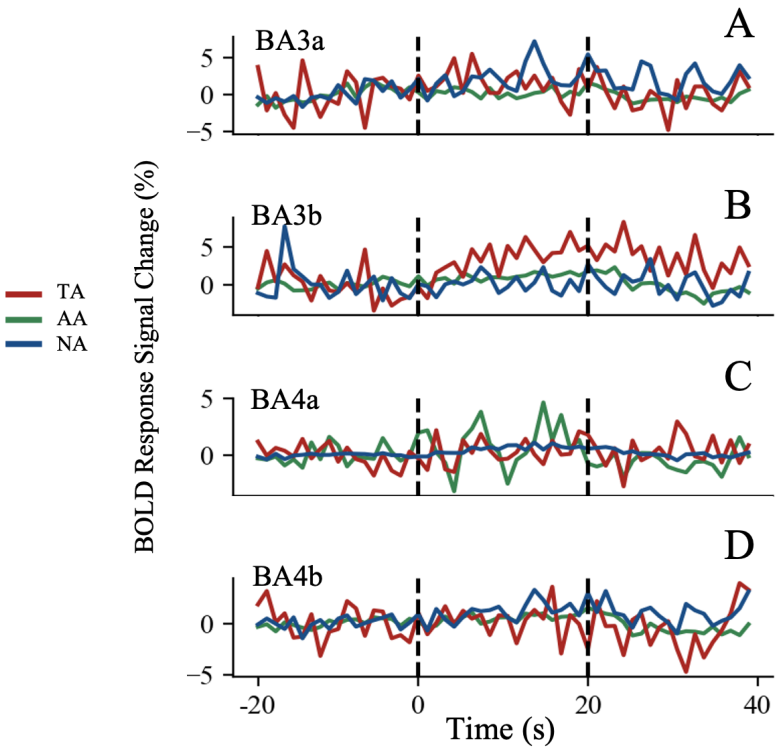

Fig S1. Functional Activation of ROI in sensorimotor areas of unaffected hemisphere. Mean percent change in the signal arising from the A) BA3a, B) BA3b, C) BA4a, D) BA4b areas of the hemisphere ipsilateral to the affected limb for each group (TA: maroon, AA: green, NA: blue). No significant difference was found between groups ($p > 0.05$, Kruskal Wallis).

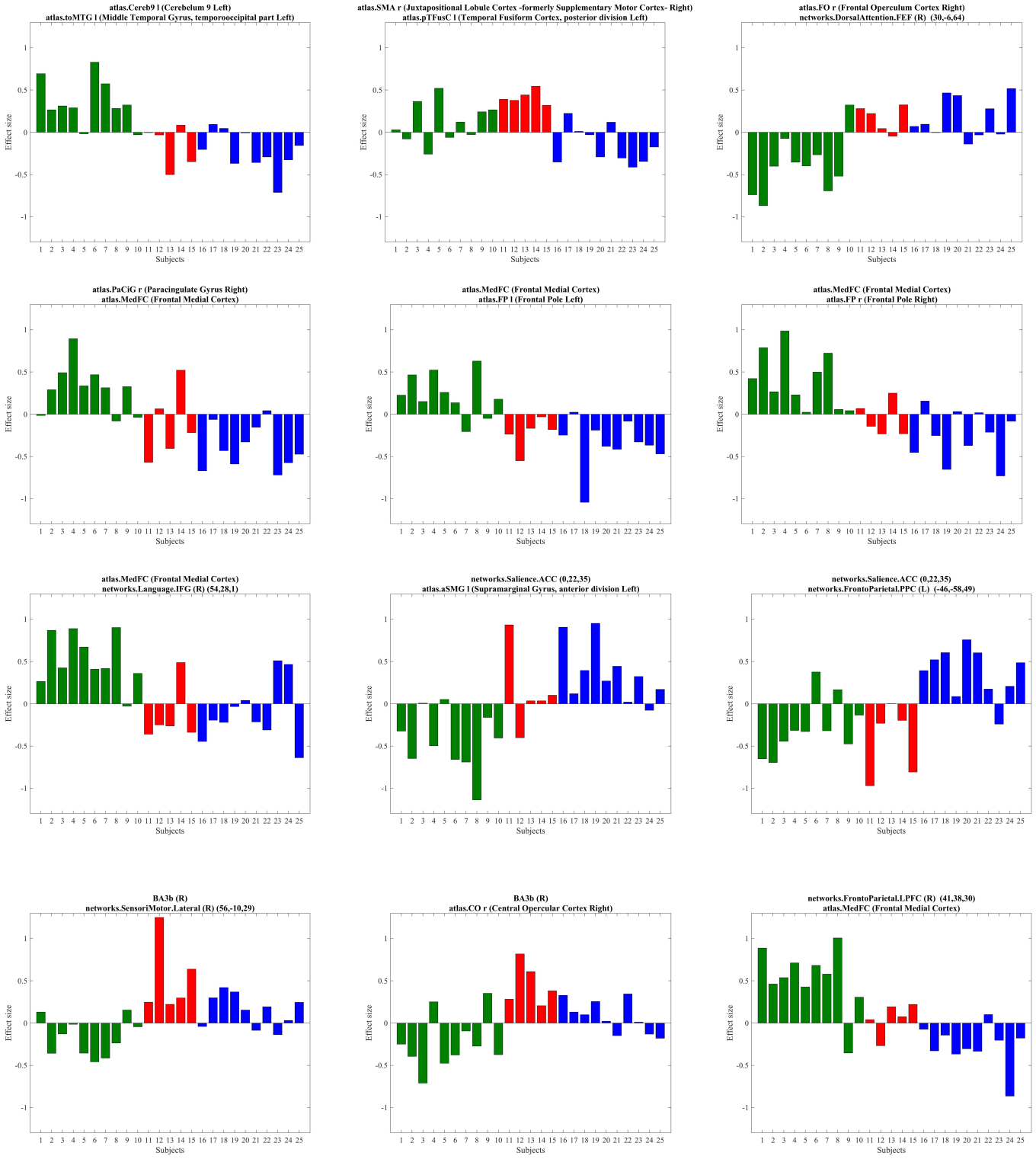

Fig. S2. Effect sizes of functional correlations. The effect size is plotted among the three groups as determined by a second-level random-effect GLM analysis at a significance threshold of a cluster corrected $p^{FDR} < 0.05$, n = 25. The condition was activation between 75% ankle movement and rest. AA: green, TA: orange, NA: blue.

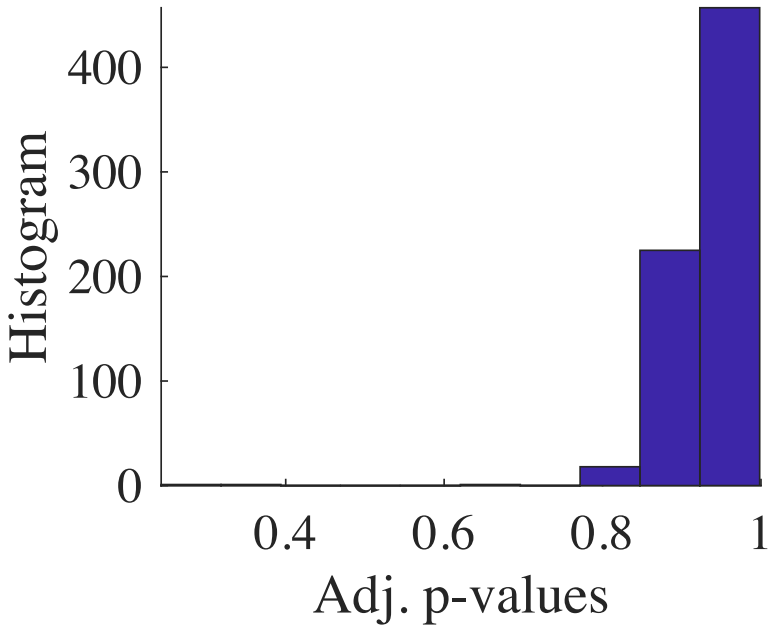

Fig. S3. Distribution of the adjusted p values for the whole-brain functional connectivity analysis comparison to phantom sensation during task. Multiple comparison correction was performed using the Benjamin-Hochberg method. The new alpha of 0.35 was determined at the fifth percentile, below which only two p values were present.

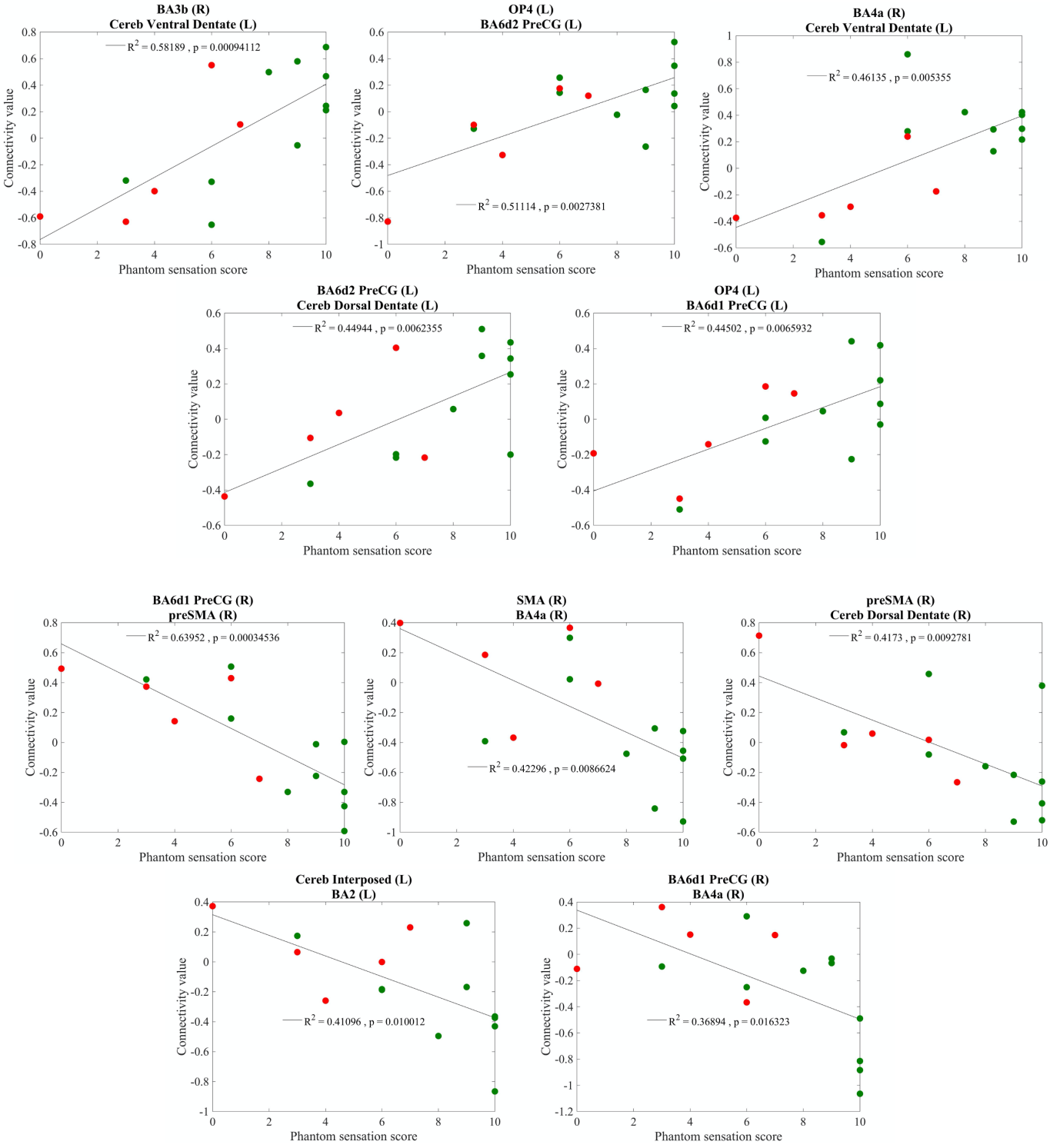

Fig. S4. Correlations for ROI-to-ROI connectivity. Individual data from the greatest positive and negative correlations are presented for ROI-to-ROI connectivity analyses correlated with phantom sensation (TA: n = 5, orange, AA: n=10, green).

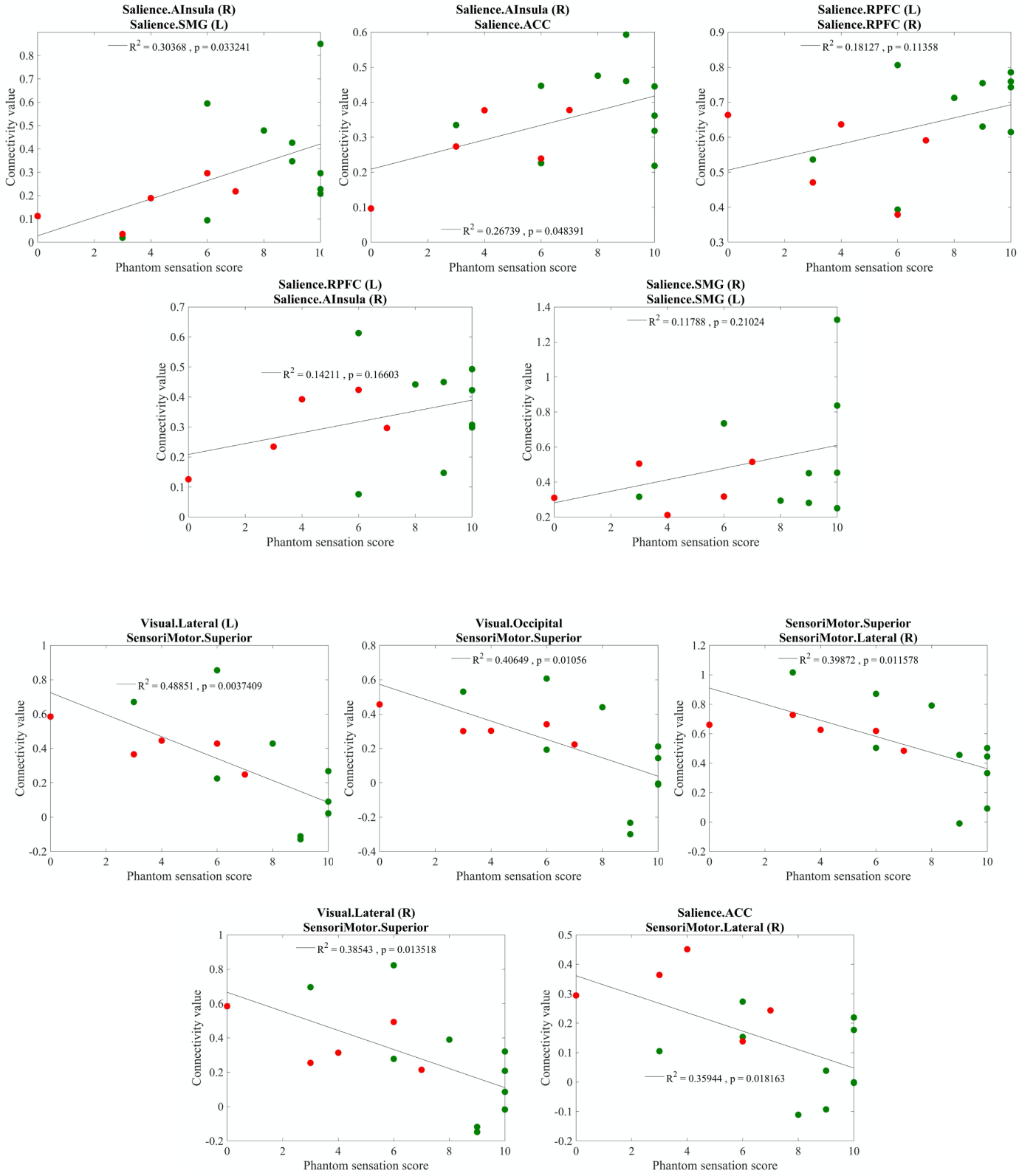

Fig. S5. Correlations for network-to-network connectivity. Individual data from the greatest positive and negative correlations are presented for network-to-network connectivity analyses correlated with phantom sensation (TA: n = 5, AA: n=10).

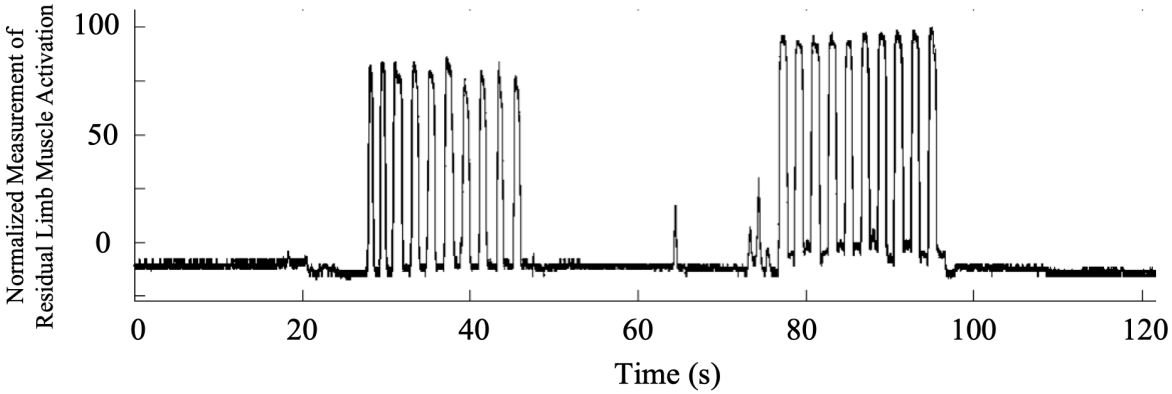

Fig. S6. Residual limb muscle activation during task. Normalized measurement of the tibialis anterior demonstrates consistent activation of the AMI musculature for 20 seconds each at two distinct levels, corresponding to the 25% ankle movement for the localizer and 75% ankle movement for the task. Representative data from one subject are provided.

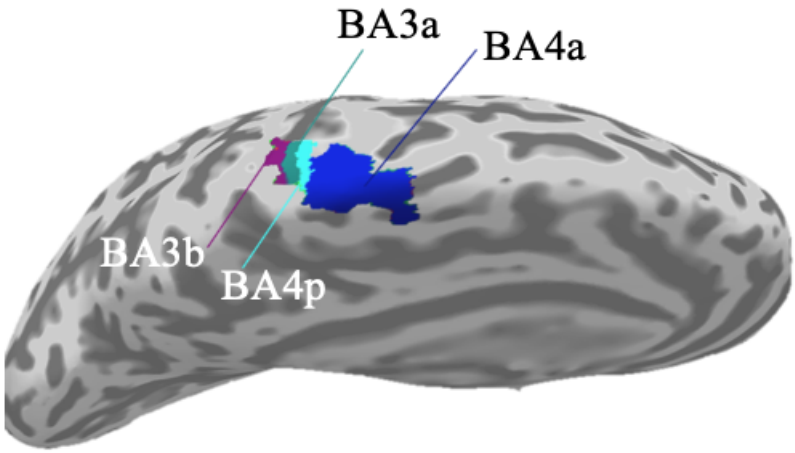

Fig. S7. ROI segmentation. ROI determination was performed to determine the active regions and subdivide them amongst the pre-defined Broadman areas (BA3a, BA4a, BA3b, and BA4p). This represents the mean ROI produced amongst all subjects.

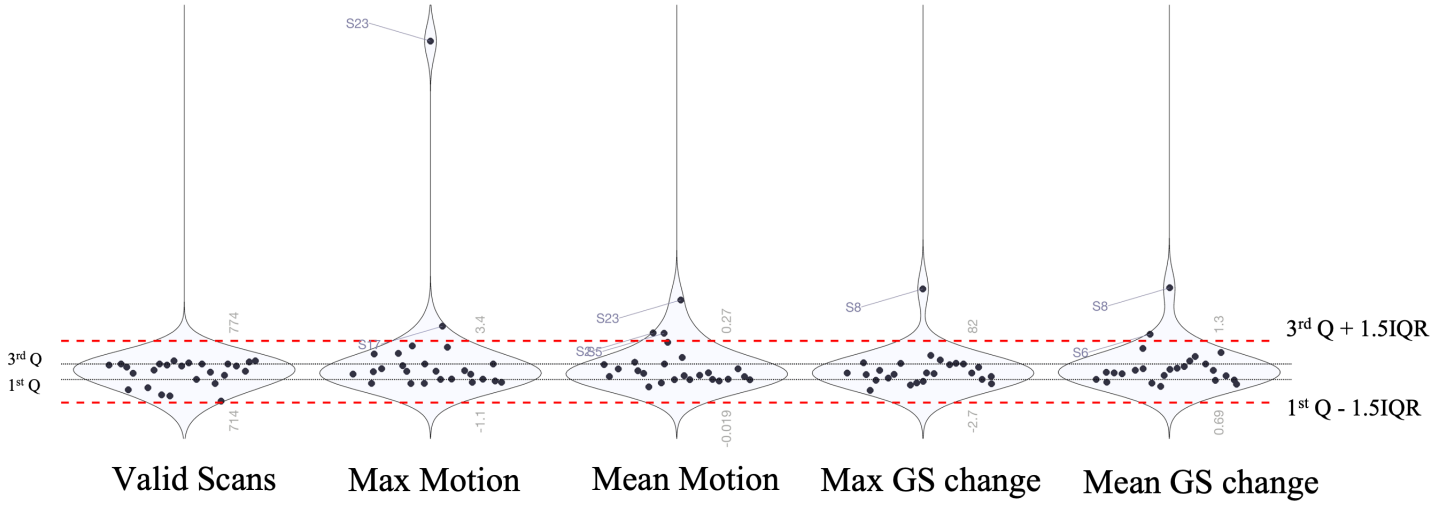

Fig. S8. Quality control histograms of motion correction parameter values across all participants. For n=25 patients, the distribution of values associated with motion during scanning is provided.

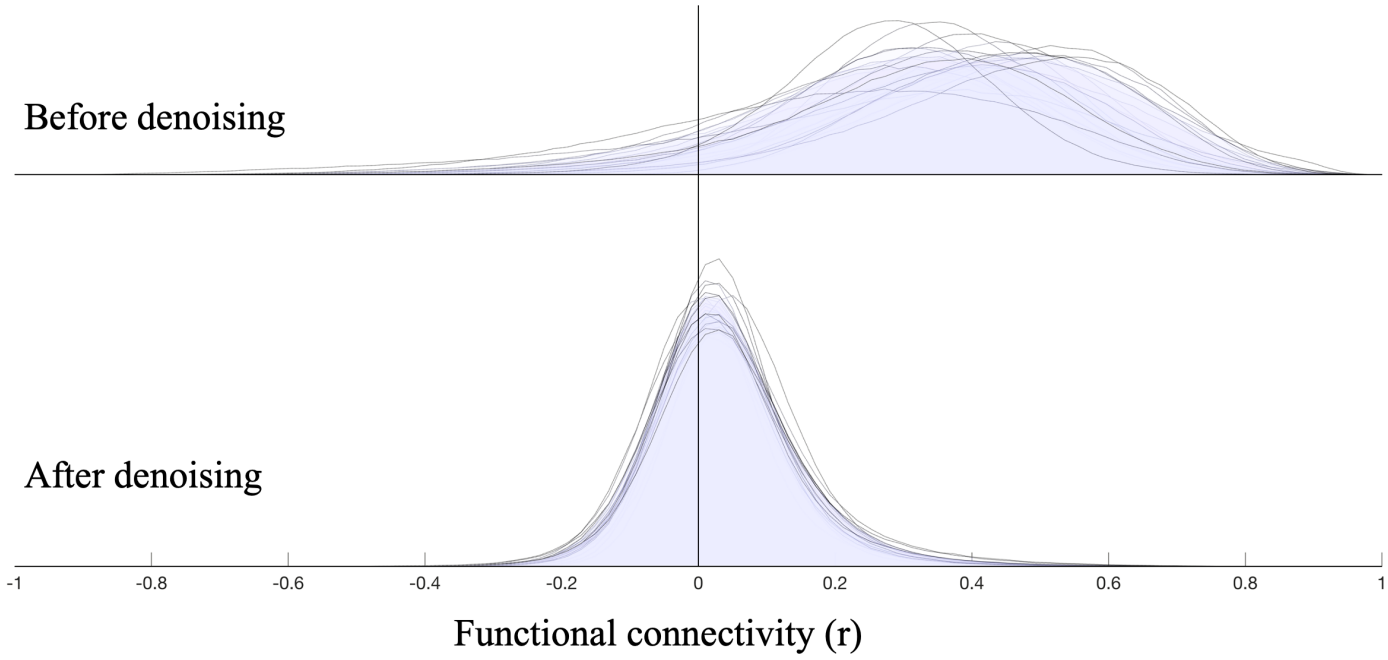

Fig. S9. Quality assurance plot of denoising. Distribution of functional correlations (Pearson correlation coefficient) across all participants before (top) and after denoising (bottom), which includes regression of white matter signals, cerebrospinal fluid signals, estimated head motion, and outliers reflecting additional structured noise sources (n=25).

Table S1. Subject demographics

Group	Amputated Side	Dominant Side	Gender	Etiology	Age at Amputation (years)	Age at scan	Amputation To Scan Time (months)
AA	L	R	M	Trauma	52	55	20
	L	R	M	Trauma	26	27	12
	R	R	M	Trauma	52	52	6
	L	R	F	Iatrogenic	65	67	10
	L	L	F	Iatrogenic	20	21	6
	L	L	F	Thermal Injury	41	42	13
	R	R	F	Trauma	28	28	6
	L	L	M	Malformity	36	37	14
	L	R	M	Trauma	52	53	17
	L	R	M	Vascular	41	42	13
	L	R	M	Trauma	26	28	18
	L	R	F	Trauma	50	52	26
TA	R	R	F	Trauma	59	61	20
	L	R	M	Malformity	23	25	24
	L	R	F	Trauma	58	59	10
	R	R	M	Trauma	58	60	23
	L	R	M	Trauma	56	58	17
	R	R	M	Trauma	36	39	30
	R	R	M	Trauma	57	59	22
NA		L	F			21	
		L	M			54	
		L	M			31	
		R	F			73	
		R	F			45	
		R	M			44	
		R	F			37	
		R	F			32	
		R	F			22	
		R	F			24	

Table S2. Individual subject data for functional activation and neuromuscular characteristics

Group	BOLD Signal Change Percentage (%)	Fascicle Strain	Position Discrimination Score
AA	0.6805	0.096	0.353
	0.2228	0.14	0.555
	0.7612	0.117	0.690
	0.9900	0.092	1.800
	0.6045	0.087	0.554
	0.9732	0.07	1.070
	0.8601	0.144	0.849
	1.6148	0.11	0.797
TA	0.3633	0.0606	
	0.7054	0.0248	0.340
	0.2333	0.0392	0.350
	0.2261	0.0398	0.380
	-0.5297	0.0223	0.000
	0.2420	0.0431	
	-0.59		
NA	0.2707		
	0.6495		
	0.4904		
	0.8612		
	0.5391		
	0.7848		
	0.7579		
	1.5843		
	1.5943		